Thermal and electrical influences from bulk plasma in cathode heating modeling

2017 Plasma Sources Sci. Technol. 26 025002

(http://iopscience.iop.org/0963-0252/26/2/025002)

IOP Publishing Plasma Sources Science and Technology

Plasma Sources Sci. Technol. **26** (2017) 025002 (14pp) doi:10.1088/1361-6595/26/2/025002

Thermal and electrical influences from bulk plasma in cathode heating modeling

Tang Chen[1], Cheng Wang[1], Xiao-Ning Zhang[2], Hao Zhang[1] and Wei-Dong Xia[1]

[1] Department of Thermal Science and Energy Engineering, University of Science and Technology of China, Hefei 230027, People's Republic of China
[2] Laboratory for Space Environment and Physical Sciences, Harbin Institute of Technology, Harbin 150001, People's Republic of China

E-mail: xiawd@ustc.edu.cn

Received 28 January 2016, revised 2 October 2016
Accepted for publication 9 November 2016
Published 23 December 2016

Abstract

In this paper, a numerical calculation is performed for the purpose of estimating the thermal and electrical influences from bulk plasma in cathode heating modeling, in other words researching the necessity of a coupling bulk plasma in near-cathode layer modeling. The proposed model applied in the present work is an improved one from previous work.

In this model, the near-cathode region is divided into two parts: the sheath and the ionization layer. The Schottky effect at the cathode surface is considered based on the analytic solution of a 1D sheath model. It is noted that the arc column is calculated simultaneously in the near-cathode region and the cathode bulk. An application is presented for an atmospheric free burning argon arc with arc currents of 50 A–600 A.

The modeling results show three interesting points: (1) at the cathode surface, energy transport due to heat conduction of heavy particles and electrons is comparable to total heating flux, no matter whether the arc discharge is performed in a high (400 A) or low current (50 A) situation; (2) the electrical influence from bulk plasma on the cathode heating modeling becomes obvious in a high current situation (>400 A) for the spot mode; (3) the near-cathode layer voltage drop (U_{tot}) is larger in the diffuse mode than in the spot mode for the same current, which is just the opposite to that for decoupled modeling.

Keywords: arc-cathode interaction, spot mode, diffuse mode, arc discharge

(Some figures may appear in colour only in the online journal)

Nomenclature

$\vec{A}$	Magnetic potential vector
A	Work function of the electrode materials
A_{eff}	Effective work function of the electrode materials
A_j	Richardson's constant
ΔA	Schottky correction to the work function
a	Stefan–Boltzmann constant
$\vec{B} = \vec{\nabla} \times \vec{A}$	Magnetic field
$\vec{C}_{\mathrm{e}}$	Average thermal speed of electrons
$C_2,\ i_{\mathrm{em}}$	Dimensionless variable for sheath calculation
D_{amb}	Ambipolar diffusion coefficient of ion
D_{e}	Electron diffusion coefficient
E_{c}	Electric field strength at the cathode surface
$\dot{E}_{\mathrm{el}}$	Rate of electron energy loss per unit volume due to elastic collisions with heavy particles
E_{i}	Ionization energy for argon gas
G	Saha function
$\vec{j}$	Current density vector
j_{bd}	Electric current delivered by back-diffusion plasma electrons
j_{em}	Thermionic emission current
j_{i}	Electric current delivered to the cathode surface by ions
j_{s}	Electric current density at the cathode surface
k_{B}	Boltzmann's constant

k_a, k_i, k_e and k_r	Thermal conductivity of atoms, ions, electrons and reactive thermal conductivity
k_{ca}	Thermal conductivity of cathode materials
$\vec{n}$	Unit vector of the cathode surface (pointing to the cathode side)
n_a, n_i	Plasma atom/ion number density
$n_{e,saha}$, $n_{a,saha}$	Number densities of the electrons and the neutral atoms under conditions of 2T Saha equilibrium
$n_{i,n}$	Ion density at the sheath edge
$n_{i,\infty}$	Ion density at the interface between the ionization layer and the thermal perturbation layer
$n_{p,n}$	Density of plasma electrons at the sheath edge
m_e, m_i, m_h	Electron/ion/heavy particle mass
p	Pressure of the gas
Q_{ea}	Collision cross section between electrons and atoms
Q_{ei}	Collision cross section between electrons and ions
q_{bd}	Energy flux delivered to the cathode surface by back-diffusion plasma electrons
q_{em}	Losses of energy due to thermionic emission
q_i	Energy flux delivered to the cathode surface by ions
q_p	Energy flux transported to electrons
q_{rad}	Thermal radiation energy loss from cathode surface
q_{tot}	Total heating flux to cathode surface
S_e	Electron energy equation source term
T_{ca}	Cathode temperature
T_e	Electron temperature
T_h	Heavy particle temperature
U_{arc}	Arc discharge voltage
U_r	Net volumetric rate of radiation loss
U_i	Voltage drop in the ionization layer
U_d	Voltage drop in the space-charge sheath
U_{tot}	Voltage drop of the near-cathode layer
$\vec{V}$	Mass-averaged velocity vector
W_i, W_e	Work of the electric field over ions and electrons in the ionization layer

Greek letters

$\alpha, \beta, \mu, \eta_c, \eta_{0,}\tau$	Dimensionless variable for the sheath/ionization layer theory
σ	Electric conductivity
ε_0	Dielectric constant
ε	Emissivity of the cathode surface
ξ_0	Permeability of vacuum
$\vec{\Gamma}_e$	Plasma electron flux
ρ	Mass density
$\vec{\tau}$	Viscous stress tensor for Newtonian fluid
μ_e	Electron mobility
υ_B	Bohm velocity
$\overline{\upsilon}_{ea}$	Average collision frequency between electrons and atoms
$\overline{\upsilon}_{ei}$	Average collision frequency between electrons and ions
φ	Electric potential field

Subsrcipt

a	Atom
amb	Ambipolar
bd	Back diffusion
c, ca	Cathode
e	Electron
em	Thermal emission
h	Heavy paticle
i	Ion
s	Sheath

1. Introduction

Unified modeling for arc plasmas and a thermionic cathode at high-pressure has long been the subject of extensive studies, thanks to the increasing power of computers. The experimental difficulties of using arc plasmas in the near-electrode region is obvious, due to the sharp change in plasma state over a very small distance [1–6]. Successful near-anode region modeling and experiments have been carried out by Tanaka, Ushio and coworkers [7–11], and Dinulescu [12]. On the other hand it has been found [13] that the near-cathode region involves highly non-linear multi-field coupling, which makes the complete simulation of arc–cathode interactions quite a time-consuming job. Thus, the near-cathode layer is not generally taken into account in many models, in which case one may just impose an arbitrary current density profile at the cathode surface [14]. Nevertheless, it is essential to develop a unified arc–cathode model for the following reasons. Experimental results have shown that there is evident arc–cathode interaction, which affects the configurations of the arc cathodic root as well as the arc column [15]. This is very useful for researching practical applications in controlling the arc column configurations and cathodic root configurations [16, 17], such as a magnetically dispersed arc plasma [18, 19], diffuse cathodic root [20], etc. To research arc discharge phenomena using a thermionic cathode, a model including the electrodes, the near-electrode layer and the arc column was successfully attempted by Lowke, Sansonnes and coworkers [21–24], Benilov, Li and coworkers [25, 26], Murphy, Schnick and coworkers [27–31].

Different models of plasma–cathode interaction in high-pressure arc discharges are systematized in [32]. To the authors' knowledge, the near-cathode layer can be treated as a region either dependent or independent of bulk plasma. In Lowke's work, the 2D non-equilibrium layer coupled with plasma was assumed to be in the local thermodynamic equilibrium state, except that effective thermal and electrical conductivities are calculated for the first mesh cells adjacent to the cathode surface [22]. The space charge layer was neglected and a 2D ionization layer was applied. In some cases of simulation [21, 22], the cathode surface temperatures seem to be in good agreement with the experimental data. However, the no-sheath approach physically conflicts with experimental facts

[25]: in low-current arcs ($I \leqslant 10$ A), the values of cathode fall are in the range of 10–50 V; in high-current arcs ($I = 50$–500 A), the cathode fall is around 4–10 V. Thus for a further study on the interaction between the arc and the cathode, a sheath-accounted approach is required. Simulations from [33] developed a novel non-equilibrium model of **a** DC electric arc, with space-charge sheaths adjacent to the electrodes. Represented by the theory of Benilov [34], those models involve both the sheath and ionization layer in a 1D description [25, 26, 34–43]. The modeling, which decouples the cathode from the plasma column, was first suggested by Bade and Yos [44] and Neumann [45], and then developed by Benilov [34, 38–40] and other researchers [3, 4, 35–37, 44–47]. These above-mentioned models included the sheath but approximately assume that the ion current fraction in the total current does not vary much under different arc column conditions. In addition, the energy balance of the near-cathode layer is assumed to be independent of the arc column. In high-pressure low-current situations (e g. high intensity discharge (HID) lamp discharge), this kind of theory is proved successfully compared to the experimental measurements [3, 4, 39, 46], and hence is widely accepted. Li, Benilov and coworkers [25, 26] tried to introduce the sheath-accounted model [39] to the high-current arc situation and prove the primary importance of near-cathode sheaths.

The basic assumptions of the decoupling method and the coupling method deviate greatly from each other. Until now, there has been no adequate strong proof for neglecting the influence of bulk plasma on the cathode arc attachment for high-pressure high-current arc discharges, e.g. cutting, welding or waste treatment. Plasma flow due to a strong magnetic field at the cathode root (the Maecker effect) could be important at high arc currents, for example, the arc root could shrink towards its tip under an external magnetic field [16]. The cathode arc attachment was shown to be greatly influenced by the plasma flowing in rotating arc simulation [15]. Further work is required to clarify whether the decoupling method is appropriate for high-current arc modeling.

Therefore in this paper, for the purpose of examining the thermal and electrical influence of bulk plasma on cathode heating, we present a two temperate arc column model coupled with 1D near-cathode layer modeling, which is developed from previous work [48]. The modeling and calculation method in this paper is basically same as a previous work [48]; however, there are several small modifications (such as the expression of electron enthalpy), and, most importantly, the electrical influence from bulk plasma on the near-cathode layer is not included in the calculation of [48]. The conduction heating flux is included in the electron energy balance equation of the ionization layer. To achieve a more accurate result, a thin thermal perturbation layer is taken into account, which is in both a chemical and thermodynamic non-equilibrium state. The thermal perturbation layer is defined as a layer in which electron thermal conduction and heating of the electrons by an ambipolar electric field are comparable to electron energy exchange in collisions with heavy particles [34, 49]. The arc model considers a tungsten rod cathode and a flat anode.

In the second part of this paper, detailed descriptions of the theory are presented. We give the descriptions of the case geometry and then a summary of the basic assumptions, the equations and boundary conditions.

In the third part, the general results of arc discharge, as current density distributions on the cathode tip, sheath voltage drop and the energy fluxes are presented.

In the last part, the summary of the main conclusions concerning the arc–cathode interaction will be presented.

2. Description of the numerical model

2.1. Concept of the coupling method

The concept of the modeling structure is illustrated in figure 1. U_i and U_d represent the voltage drop in the ionization layer/sheath layer; U_{arc} represents the whole arc discharge voltage; U_{cl} represents bulk plasma voltage drop. In our previous work, the electrical influence from the bulk plasma on the near-cathode layer was not included in the calculation [48] (this means $U_i + U_d$ is uniform in the cathode arc attachemnt), however in our present work $U_{arc} = U_d + U_i + U_{cl}$ is assumed to be uniform, giving a certain total current. The idea that Ohm's law should be included in the near-cathode layer modeling, which leads to cathode voltage drop variation along the cathode surface, is not new. This idea has been developed in a series of works by Nemchinsky [3, 46, 50–53]. The basic assumptions for each layer introduced are summarized in table 1. The plasma region in front of the hot cathode is divided into three subzones [49, 54]: a space-charge sheath, an ionization layer, and a layer of thermal perturbation (or thermal relaxation). The thermal perturbation layer is established for the purpose of introducing the arc column's influence on the near-cathode layer. This layer is assumed to be a thin layer with length 200 μm, between the near-cathode layer and the arc column. Alternatively, one can take this layer as a part of the arc column. The basic assumptions taken for the thermal perturbation layer are summarized as follows: (a) the layer is in the thermal non-equilibrium and chemical non-equilibrium state; (b) the layer is a flow-affected 2D region; (c) the layer is supposed to be in a quasi-neutral state, which leads to an ambi-polar diffusion approximation for the calculation of electron number density.

As table 1 shows, these zones may be characterized by the following length scales, respectively: the length of electron energy relaxation λ_u; the ionization length λ_i; the Debye length λ_D [34]. The length of electron energy relaxation λ_u is defined as a length scale on which electron thermal conduction and heating of the electrons by the ambipolar electric field are comparable to electron energy exchange in collisions with heavy particles [34]; the ionization length λ_i represents a distance to the cathode surface in which deviations from ionization equilibrium are validated.

The typical modeling of plasma boundary layer of high intensity discharge (HID) cathodes [47], maintains that the cathodic plasma boundary layer in front of a thermionically emitting cathode is independent of the bulk plasma. Following this idea the current transfer and power flux density across the boundary layer is locally 1D and governed by local values of the cathode temperature T_{ca} and of the voltage U_{tot} applied to the ionization layer and the sheath [34]:

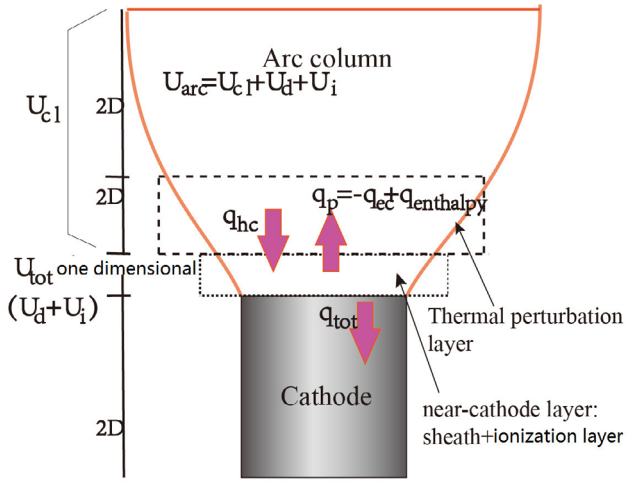

Figure 1. Schematic diagram of the coupled modeling.

Table 1. The basic assumptions.

		Dimension	assumptions
1	Sheath	$\lambda_D \sim 0.1\,\mu$m, 1D	$n_e \neq n_i$, collisionless, $T_e \neq T_i$
2	Ionization layer	$\lambda_i \sim 10\,\mu$m, 1D	$n_e = n_i$, $T_e \neq T_i$
3	Thermal perturbation layer	$\lambda_u \sim 200\,\mu$m, 2D	$n_e = n_i$, $T_e \neq T_i$, flow-affected
4	Arc column	$l \sim 5$ mm, 2D	$n_e = n_i = n_{saha}$, $T_e \neq T_i$

$$j_s(T_e,\ U_{tot}) = j_i - j_{bd} + j_{em} \tag{1}$$

$$q_{tot}(T_e,\ U_{tot}) = j_s\left(U_{tot} - A_{eff} - (2.5+0.7\delta)\frac{k_B T_e}{e}\right) - q_{rad} \tag{2}$$

where j_{em} is the density of the thermionic emission current, j_i is the density of the electric current delivered to the cathode surface by ions, j_{bd} is the density of the electric current from the cathode to the plasma transported by back-diffusion plasma electrons, A_{eff} is the effective work function of the electrode materials, T_e is the local electron temperature, $q_{rad} = \varepsilon a T_{ca}^4$ represents the radiation energy losses (ε, emissivity of the cathode surface; a, Stefan–Boltzmann constant), and δ is a correction term proportional to the ionization degree $\delta = \frac{n_e}{n_i + n_a}$, which has to be added to the electron enthalpy flow in the case of a high degree of ionization [47]. The total voltage drop of the near-cathode layer $U_{tot} = U_d + U_i$.

As is known, for decoupled modeling the contribution of heat conduction to the electron power balance of the boundary layer is neglected. In this work, thermal conduction heating by heavy/electron particles is evaluated using $q_{hc} = -k_h \vec{\nabla} T_h \cdot \vec{n}$ and $q_{ec} = -k_e \vec{\nabla} T_e \cdot \vec{n}$. Here, $\vec{n}$ represents the unit vector of the boundary surface (pointing to the cathode side). The expressions for the cathode heating flux components are [34, 39, 40]:

$$q_i = \frac{j_i}{e}(eU_s + E_i - A_{eff}) + W_i;$$

$$q_{bd} = \frac{j_{bd}}{e}(2k_B T_e + A_{eff});\quad q_{em} = -\frac{j_{em}}{e}(2k_B T_{ca} + A_{eff})$$

where q_i and q_{bd} are the densities of energy fluxes delivered to the cathode surface by ions and by back-diffusion plasma electrons, q_{em} is the density of losses of energy by the cathode surface due to thermionic emission, and E_i is the ionization energy for argon gas.

Thus equation (2) is rewritten as:

$$q_{tot} = j_s\left(U_{tot} - A_{eff} - (2.5+0.7\delta)\frac{k_B T_e}{e}\right) - q_{rad} - k_e \vec{\nabla} T_e \cdot \vec{n} - k_h \vec{\nabla} T_h \cdot \vec{n} \tag{3}$$

and the electron energy balance equation in ionization layer is rewritten as:

$$\frac{j_{bd}}{e}(2k_B T_e + eU_s - \Delta A) + E_i\frac{j_i}{e} + k_e \vec{\nabla} T_e \cdot \vec{n} + k_h \vec{\nabla} T_h \cdot \vec{n} + (2.5+0.7\delta)\frac{k_B T_e}{e} j_s = \frac{j_{em}}{e}(2k_B T_{ca} + eU_s - \Delta A) + W_e \tag{4}$$

where W_e [39] is the work of the electric field over electrons, $W_e = j_s U_i - 0.5 j_i U_i$, following [38, 39]. $\Delta A = \sqrt{\frac{e^3 E_c}{4\pi\varepsilon_0}}$ is the Schottky correction to the work function. Note that [38, 39] did not include ΔA in the electron energy balance while other simulations such as [47] did. Though the results with and without the ΔA term (in equation (4)) are virtually the same, we suggest in future that the related simulation does not include the ΔA term, because the equation with the ΔA term implies that there is a cathode voltage drop with a zero electric field at the cathode surface, which is not physically acceptable.

Therefore the total energy flux transported to electrons q_p, at the near-cathode layer boundary is evaluated as (using equation (4)):

$$q_p = k_e \vec{\nabla} T_e \cdot \vec{n} + (2.5+0.7\delta)k_B T_e j_s = \frac{j_{em}}{e}(2k_B T_{ca} + eU_s - \Delta A) + W_e - \frac{j_{bd}}{e}(2k_B T_e + eU_s - \Delta A) - E_i\frac{j_i}{e}. \tag{5}$$

The detailed expressions for each component of current density are given in appendix A.

2.2. Conservation equations

2.2.1. Arc column and thermal perturbation region. In this work, the arc column is of the axisymmetrical two-temperature type. Therefore the energy equations are general in both the arc column and the thermal perturbation region.

Continuity equation:

$$\vec{\nabla} \cdot (\rho \vec{V}) = 0. \tag{6}$$

Momentum conservation equation:

$$\rho(\vec{V} \cdot \vec{\nabla})\vec{V} = \vec{\nabla} \cdot (-p\vec{I} + \vec{\tau}) + \vec{j} \times \vec{B}. \tag{7}$$

Here $\vec{V}$, ρ and p are the mass-averaged velocity, density and pressure of the gas, respectively, $\vec{I}$ is the identity matrix, $\vec{\tau}$ denotes the viscous stress tensor for Newtonian fluid, and $\vec{j}$ and $\vec{B}$ are the current density and magnetic field.

The heavy particle energy conservation equation is:

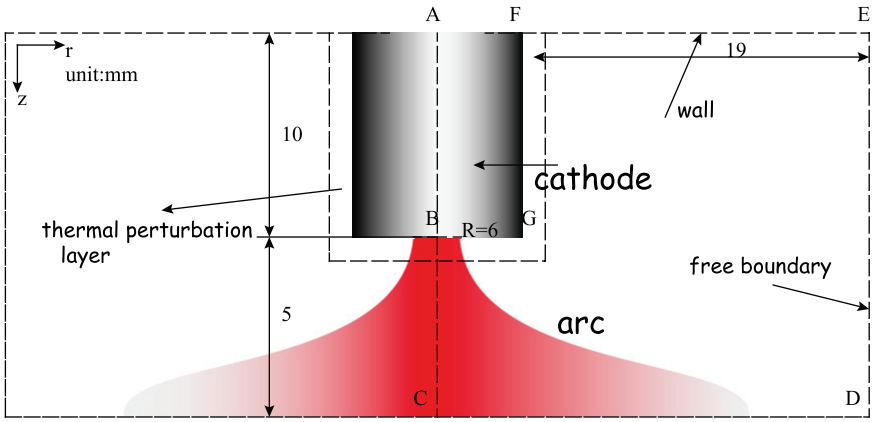

Figure 2. Schematic view of the computational domain.

Table 2. Boundary conditions.

Boundary	T_e	T_h	P	$\vec{V}$	φ	$\vec{A}$	n_i
E–F	1000 K	300 K	—	0	$\frac{\partial\varphi}{\partial n}=0$	$\frac{\partial\vec{A}}{\partial n}=0$	—
D–E	$\frac{\partial T_e}{\partial n}=0$ (if backflow: 1000 K)	$\frac{\partial T_h}{\partial n}=0$ (if backflow: 1000 K)	$\frac{\partial P}{\partial n}=0$	$\frac{\partial\vec{V}}{\partial n}=0$	$\frac{\partial\varphi}{\partial n}=0$	$\frac{\partial\vec{A}}{\partial n}=0$	—
C–D	Flux = 0	1000 K	—	0	$\varphi=0$	$\frac{\partial\vec{A}}{\partial n}=0$	—
B–G–F	Flux = q_p	$T_h=T_{ca}$	—	0	$j=-j_s$ (plasma side) $j=j_s$ (cathode side)	coupled	$Flux=-n_i\upsilon_B$
A–F	—	300 K	—	—	$\varphi=0$	$\frac{\partial\vec{A}}{\partial n}=0$	—

$$\vec{\nabla}\cdot\left[-(k_a+k_i+k_r)\vec{\nabla}T_h+\frac{5}{2}(n_a+n_i)k_BT_h\vec{V}\right]=\dot{E}_{el}. \quad (8)$$

The electron energy conservation equations [26]:

$$\vec{\nabla}\cdot\left(-k_e\vec{\nabla}T_e+\left(\frac{5}{2}+0.7\delta\right)k_BT_e\vec{\Gamma}_e+n_iE_i\vec{V}\right)=-\dot{E}_{el}+S_e \quad (9)$$

$$S_e=\vec{j}\cdot\vec{E}-U_r \quad (10)$$

$$\dot{E}_{el}=\frac{2m_e}{m_h}(\overline{\upsilon}_{ea}+\overline{\upsilon}_{ei})n_e\frac{3}{2}k_B(T_e-T_h) \quad (11)$$

where T_h, T_e, k_a, k_i, k_r, and k_e represent the heavy particle temperature, electron temperature, thermal conductivity of atoms, thermal conductivity of ions, reactive thermal conductivity, and thermal conductivity of electrons, respectively. The thermal conductivity for the heavy particle energy equation is $k=k_a+k_i+k_r$. $\dot{E}_{el}$ is the energy transferred in elastic collisions between electrons and heavy particles, which can be expressed as equation (11) shows. In particular, the electron flux $\vec{\Gamma}_e$ is set to $n_e\vec{V}-\frac{\vec{j}}{e}$ in the arc column region. S_e, U_r, $\overline{\upsilon}_{ea}$, and $\overline{\upsilon}_{ei}$ represent the electron energy equation source term, net volumetric rate of radiation loss, average collision frequency between electrons and atoms, and average collision frequency between electrons and ions.

$$\overline{\upsilon}_{ea}=\overline{C}_en_aQ_{ea} \quad (12)$$

$$\overline{\upsilon}_{ei}=\overline{C}_en_iQ_{ei} \quad (13)$$

$$\overline{C}_e=\sqrt{\frac{8k_BT_e}{\pi m_e}} \quad (14)$$

where $\overline{C}_e$, Q_{ea}, Q_{ei}, n_a, n_i, k_B, and m_e represent the average thermal speed of electrons, collision cross section between electrons and atoms, collision cross section between electrons and ions, atom number density, ion number density, Boltzmann constant and the electron mass, respectively.

The electric potential and magnetic vector potential equations are:

$$\vec{\nabla}\cdot(-\sigma\vec{\nabla}\varphi+eD_e\vec{\nabla}n_e)=0 \quad (15)$$

$$\vec{\nabla}^2\vec{A}=-\xi_0\vec{j} \quad (16)$$

$$\vec{B}=\vec{\nabla}\times\vec{A},\ \vec{j}=-\sigma\vec{\nabla}\varphi+eD_e\vec{\nabla}n_e \quad (17)$$

where σ represents the electric conductivity, and ξ_0 is the permeability of vacuum. The electric potential and magnetic vector potential equations are solved in the arc column region, ionization layer and cathode region. The second right-hand term of $\vec{j}$, $eD_e\vec{\nabla}n_e$ is only calculated in the thermal perturbation layer. D_e, the electron diffusion coefficient, is evaluated as $\sigma\frac{k_BT_e}{n_ee}$.

2.2.2. Ion/electron particle flux in the thermal perturbation layer. In the arc column, electrons and the neutral atoms are evaluated under conditions of 2T Saha equilibrium. In the

thermal perturbation layer, based on the assumptions mentioned in section 2.1, we apply the drift-diffusion approximation; the electron flux reads: $\vec{\Gamma}_e = -D_e \vec{\nabla} n_e - \mu_e n_e \vec{E} + n_e \vec{V}$ [55]. In our 2D thermal perturbation layer, the quasi-neutrality state of the plasma is assumed, and primary ions/electrons and atoms are taken into account. Then, the electron and ion flux can be calculated approximately as: $\vec{\Gamma}_e = -D_{amb} \vec{\nabla} n_e + n_e \vec{V} - \frac{\vec{j}}{e}$ and $\vec{\Gamma}_i = -D_{amb} \vec{\nabla} n_i + n_i \vec{V}$. This leads to the solution of the ambipolar diffusion equation:

$$\vec{\nabla} \cdot (-D_{amb} \vec{\nabla} n_i + n_i \vec{V}) = \dot{n}_i. \quad (18)$$

The net ionization rate is $\dot{n}_i = \alpha_{re}(G n_e n_a - n_e^3)$, G is the Saha function $G = n_{e,saha}^2 / n_{a,saha}$, $n_{e,saha}$ and $n_{a,saha}$ are, respectively, the number densities of the electrons and the neutral atoms under conditions of 2T Saha equilibrium, the three-body recombination coefficient α_{re} is taken from [21], the ambipolar diffusion coefficient D_{amb} is calculated from the method of [56], and σ in the thermal perturbation layer is expressed as: $\sigma \approx \sigma_e = \frac{e^2 n_e}{m_e \nu_e}$, where the electron collision frequency $\nu_e = \overline{\upsilon}_{ea} + \overline{\upsilon}_{ei}$.

2.2.3. Cathode body. Heat transfer equation is solved in the cathode body and reads:

$$\vec{\nabla} \cdot (-k_{ca} \vec{\nabla} T_{ca}) = \vec{j} \cdot \vec{E} \quad (19)$$

where k_{ca} represent the thermal conductivity of cathode materials, and T_{ca} is the cathode temperature.

In the cathode body the electric potential and magnetic vector potential equations are same as those given in 2.2.1

2.3. Calculation domain and boundary conditions

In this study, the free burning argon arc configuration is simplified as schematically shown in figure 2. A dc argon arc burns between a pure tungsten rod cathode and a flat anode. The diameter of the cathode is 12 mm, while the length of it is 10 mm, which corresponds to the literature [38]. The boundary conditions of the primary variables are summarized in table 2. At the axis of symmetry (*A–B–C*) of the domain, the axial symmetric conditions are employed. *E–F* is the wall, where a uniform temperature ($T_h = 300$ K, $T_e = 1000$ K) is assumed. At *A–F*, the cathode bottom, the electric potential is set to be zero and the temperature is assumed to be uniform (300 K) as previous work [38] did. *C–D* is the anode bottom, where the temperature is set to be 1000 K and the electric potential is set to be zero. At the outlet *D–E*, a zero gradient of each primary variable is imposed with a backflow gas of a constant temperature (1000 K). Though at outlet some simulations [14, 57] introduce conditions of $\frac{\partial T_e}{\partial n} = 0$ in spite of backflow, the differences are small and limited in the near-outlet area.

At *B–G–F*, the plasma/cathode interface, there are in fact two interfaces. One is the interface between the cathode and sheath: the normal component of the electric current density is continuous; the heating flux to cathode is set as q_{tot}; the heavy-particle temperature equals the cathode surface temperature. The other one is the interface between the ionization layer and the thermal perturbation layer: for the electron energy equation, a heating flux of: $q_n = k_e \vec{\nabla} T_e \cdot \vec{n} + (2.5 + 0.7\delta) k_B T_e j_s = \frac{j_{em}}{e}(2k_B T_{ca} + eU_s - \Delta A) + W_e - \frac{j_{bd}}{e}(2k_B T_e + eU_s - \Delta A) - E_i \frac{j_i}{e}$ is applied (derived from equation (5)); following works [26, 57], the heavy-particle temperatures and the normal component of the electric current density are continuous. Bohm's criterion (υ_B is the Bohm velocity, see equation (A.2) in appendix A) is adopted for the sheath/ionization layer boundary, which is explained in appendix A. The boundary condition $\frac{\partial n_i}{\partial n} = 0$ is used for the ion density calculation (2D) on the bulk plasma side, because we assume that the ion diffusion flux towards the cathode surface is majorly influenced by the ionization layer ion number density gradient (which is treated as 1D), and calculated using the equations from [34].

3. Results and discussions

Governing equations are solved in FLUENT software using the SIMPLE algorithm. The transport properties of argon were calculated by Zhang [58].

3.1. Heating of the thermionic cathode

In the present work, two stable modes of solution (diffuse mode and spot mode) are obtained for arc currents 50–600 A. The two different types of cathode modes (diffuse and spot) were first obtained in [59]. Radial variation of the cathode voltage drop was also taken into account in this work and the following ones [3, 46, 50–53]. The two different modes are obtained from different initial conditions. In the calculation, the cathode arc attachment in the spot mode is limited in $S < 6$ mm and when $S > 6$ mm we introduce $\frac{\partial T_e}{\partial n} = 0$ as the boundary condition for the electron energy equation. The cathode surface temperature/electron temperature along *B–G–F* is illustrated in figure 3 for $I = 50$ A, 200 A, 400 A. In figure 3, '*S*' represents the distance from the center of the cathode head measured along the generatrix. The maximum cathode temperature appears in the cathode head fringe (G) for diffuse mode and in cathode head center (B) for the spot mode, where the total current density also reaches its maximum (figures 4 and 5). The maxium value of the cathode temperature reaches 3940 K, 3961 K, 3973 K for arc current 50 A, 200 A, 400 A in spot mode, and 3367 K, 3668 K, 3794 K in diffuse mode. The electron temperature in the diffuse mode is much lower than that in the spot mode. The maxium value of electron temperature reaches 30 499 K, 31 117 K, 33 007 K for arc current 50 A, 200 A, 400 A in spot mode and 18 934 K, 19 608 K, 17 944 K in diffuse mode. However, it has been reported in previous numerical work [38, 39] that the spot mode of an arc discharge has two branches: there exists a solution of the spot mode in which both the center and fringe of the cathode head has a temperature peak. The present work could not obtain a stable second spot mode of the arc discharge; this is caused by a numerical problem, because, as

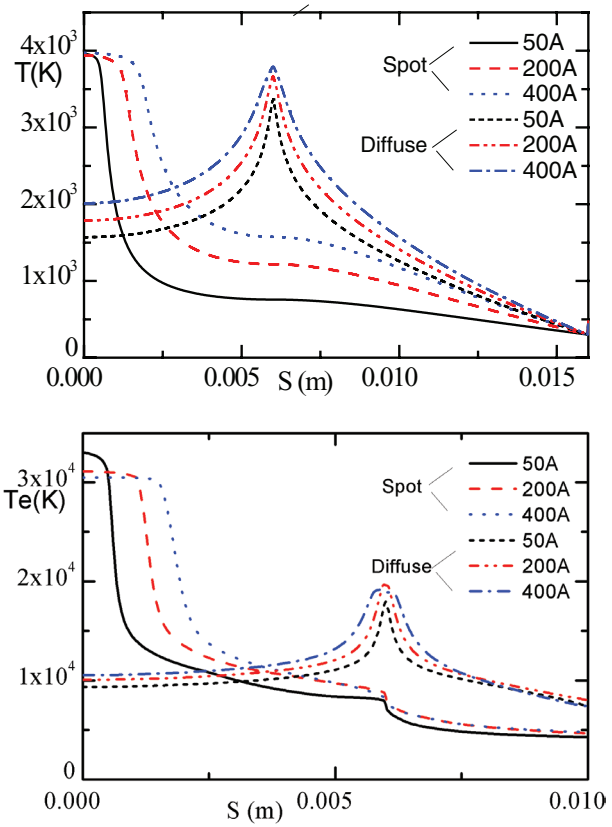

Figure 3. Cathode surface temperature/electron temperature distribution along *B–G–F*, for different arc currents: $I = 50$ A, 200 A, 400 A.

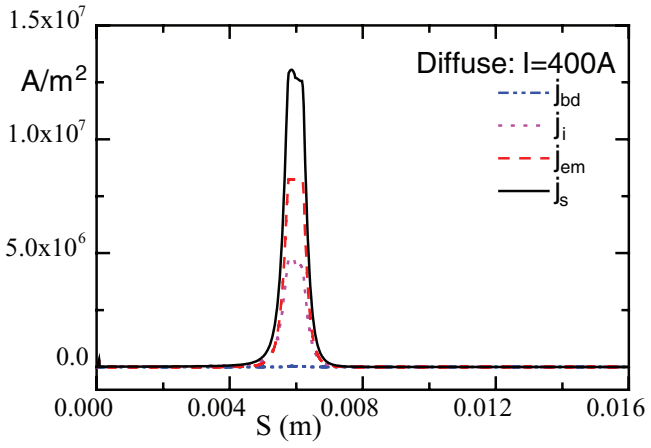

Figure 4. Distributions of total current density j_s and its components (ion current density j_i, electron back diffusion current density j_{bd} and electron thermal emission current density j_{em}) along the cathode surface B–G–F: diffuse mode, $I = 400$ A.

indicated in paper [60], a discharge mode can join another mode or turn back, but not terminate suddenly.

Distributions of total current density j_s and its components (ion current density j_i, electron back diffusion current density j_{bd} and electron thermal emission current density j_{em}) along the cathode surface B–G–F, are plotted in figures 4 and 5 for $I = 400$ A. The maximum of the total current density is equal to 1.31×10^7 A m^{-2} and 4.34×10^7 A m^{-2} for the diffuse mode and spot mode, respectively. The maximum of the ion current density is equal to 4.85×10^6 A m^{-2} and 9.87×10^6 A m^{-2} for the diffuse mode and spot mode, respectively. As shown in figures 4 and 5, for the diffuse mode the electron back diffusion current is negligible in most areas; for the spot mode, the electron back diffusion current is about half of the ion current density. Thus we can approximately suppose $j_{tot} \approx j_{em} + j_i$ for the diffuse mode.

The total heating flux to cathode surface (q_{tot}) and its components (the densities of energy fluxes delivered to the cathode surface by ions q_i, by back-diffusion plasma electrons q_{bd}, by emission electrons q_{em}, and by radiation q_{rad}) along the cathode surface are shown in figures 6 and 7, for $I = 400$ A. The maximum of the total heating flux is equal to 9.64×10^7 W m^{-2} and 2.07×10^8 W m^{-2} for the diffuse mode and spot mode, respectively. The maximum of its ion heating component is equal to 1.53×10^8 W m^{-2} and 3.04×10^8 W m^{-2} for the diffuse mode and spot mode, respectively. For the diffuse mode, the maximum value of each heating flux is located at the fringe of the cathode head, where the temeprature and current density also reach a maximum. However, for the spot mode the maximum value of the total heating flux is located at $S = 1.75$ mm, while the maximum temperature appears in the center of the cathode. As figures 6 and 7 show, the electron thermal emission has a much more obvious cooling effect on the cathode than thermal radiation; The plasma back-diffusion electron heating is nearly zero in the diffuse mode, but nevertheless has quite an important role in the spot mode of the arc discharge.

The calculations of q_{bd}, q_{em}, q_i and q_{rad} are the same as the decoupled method of Benilov [39], however in the present work thermal condution from the plasma is taken into account and the contribution of the thermal conduction part is shown in section 3.2 for the convenience of discussion and reading.

3.2. Thermal influence from the bulk plasma

The typical 'decoupled' methods of cathode heating modeling [34, 37, 47] assume that the influence of the bulk plasma on the boundary layer can be neglected. However in this paper, the density of the net energy flux to the cathode surface generated in the near-cathode region is evaluated considering the influence of thermal conduction from bulk plasma. The densities of energy fluxes due to heat conduction of heavy particles (q_{hc}), electrons (q_{ec}) and the electron enthalpy transport ($q_{enthalpy}$) are plotted in figures 8 and 9 for $I = 50$ A and figures 10 and 11 for $I = 400$ A. The expressions of each energy flux component are: $q_{hc} = -k_h \vec{\nabla} T_h \cdot \vec{n}$; $q_{ec} = -k_e \vec{\nabla} T_e \cdot \vec{n}$; $q_{enthalpy} = (2.5 + 0.7\delta)\frac{k_B T_e}{e} j_s$.

For $I = 50$ A, the maximum absolute value of q_{tot}, q_{hc} and q_{ec} reaches 2.08×10^8 W m^{-2}, 6.26×10^7 W m^{-2} and 1.66×10^8 W m^{-2} in dffuse mode, and 5.93×10^8 W m^{-2}, 9.61×10^7 W m^{-2} and 1.02×10^9 W m^{-2} in spot mode, respectively. For $I = 400$ A, the maximum absolute value of q_{tot}, q_{hc} and q_{ec} reaches 9.67×10^7 W m^{-2}, 8.80×10^7 W m^{-2} and 1.31×10^8 W m^{-2} in dffuse mode, and 2.07×10^8 W m^{-2},

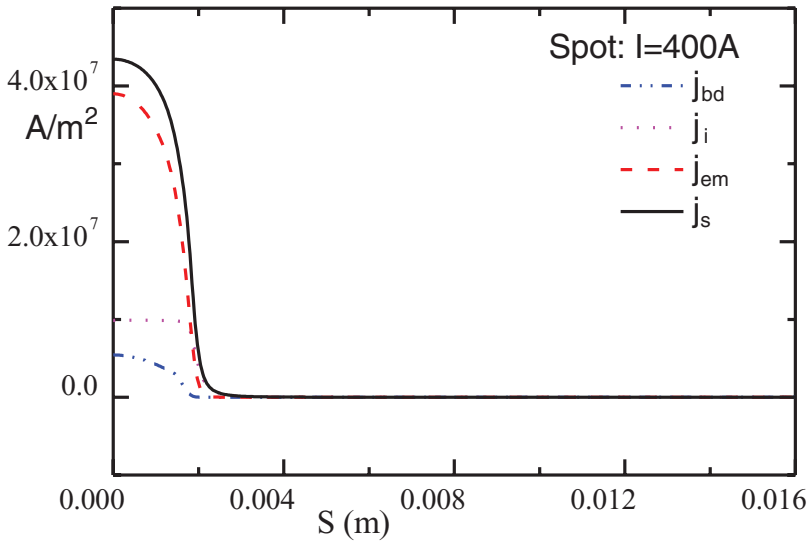

Figure 5. Distributions of total current density j_s and its components along cathode surface B–G–F: spot mode, $I = 400$ A.

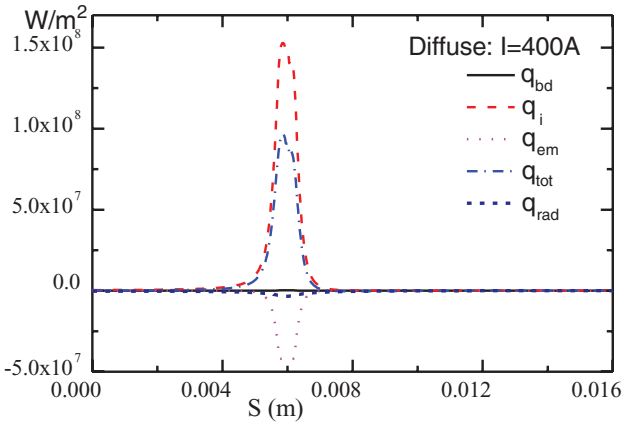

Figure 6. Distributions of the total heating flux to cathode surface (q_{tot}) and its components (the densities of energy fluxes delivered to the cathode surface by ions q_i, by back-diffusion plasma electrons q_{bd}, by emission electrons q_{em}, and by radiation q_{rad}) along the cathode surface B–G–F: diffuse mode, $I = 400$ A.

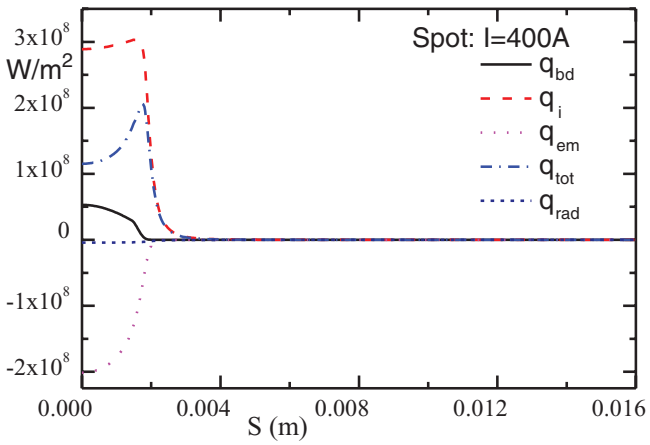

Figure 7. Distributions of the total heating flux to cathode surface (q_{tot}) and its components along the cathode surface B–G–F: spot mode, $I = 400$ A.

9.76×10^7 W m^{-2} and 1.70×10^8 W m^{-2} in spot mode, respectively.

Therefore as figures 8–11 show, no matter whether in a low current (50 A) or a high current (400 A) situation, the energy fluxes due to heat conduction of heavy particles and electrons are not negligible ones. Nor is the sum of them. This conclusion is in agreement with simulations from [32]. The thermal condution from the bulk plasma is as important as the electron enthalpy transport. At the same time the figures indicate that a substantial part of the electric power generated in the near-cathode layer is transported to the the arc column (equals $q_{enthalpy} - q_{ec}$), which is also justified in decoupled numerical calculations [26].

3.3. Electrical influence from bulk plasma

As mentioned in the introduction, decoupled modeling of cathode heating also assumes that the voltage dop of the near-cathode layer ($U_{tot} = U_i + U_d$) is uniform in the whole arc root attachment [25]. This assumption stands on the condition that the voltage drop of the bulk plasma does not vary much around the arc root attachment. In figures 12–15 each voltage drop distribution is illustrated along the cathode surface for $I = 50$ A, 400 A: U_d represents the sheath layer voltage drop; U_i represents the ionization layer voltage drop; U_{cl} represents bulk plasma voltage drop, i.e. the absolute value of the plasma potential; U_{tot} is the near-cathode layer voltage drop, which equals the sum of U_i and U_d.

For the low current (50 A) situation, the variation of the bulk plasma voltage drop is very limited (~0.3 V) in the diffuse mode and a small value (~4 V) in the spot mode. Considering the fact that the voltage drop of the near-cathode layer U_{tot} is as large as ~50 V, we can approximately suppose that U_{tot} is uniform in the whole arc root attachment. However, for the high current (400 A) situation, the variation in the bulk plasma voltage drop reaches ~1.8 V in the diffuse mode and ~7 V in the spot mode. Therefore, it is physically inappropriate to

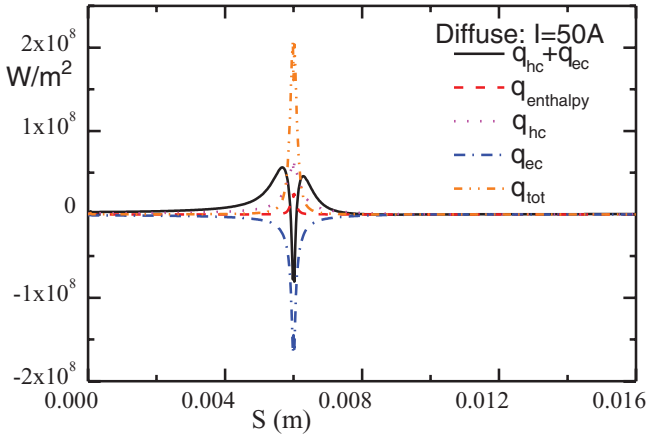

Figure 8. Distributions of the energy flux densities along the cathode surface B–G–F for arc current $I = 50$ A, diffuse mode; q_{hc}, q_{ec} and $q_{enthalpy}$ represent the densities of the energy fluxes due to heat conduction of heavy particles, electrons and the electron enthalpy transport; q_{tot} represents the total heating flux to the cathode surface.

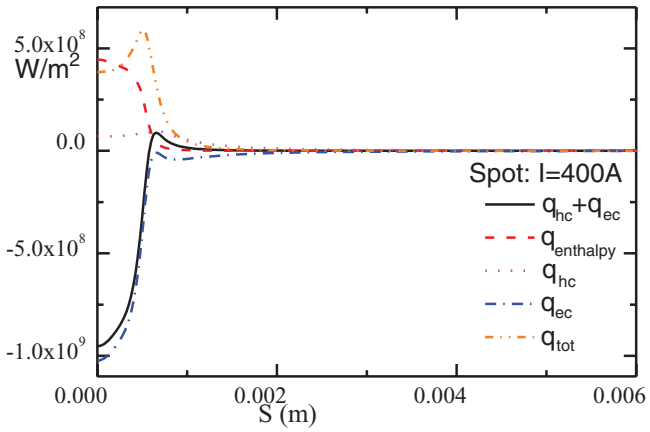

Figure 9. Distributions of the energy flux densities along the cathode surface B–G for arc current $I = 50$ A, spot mode.

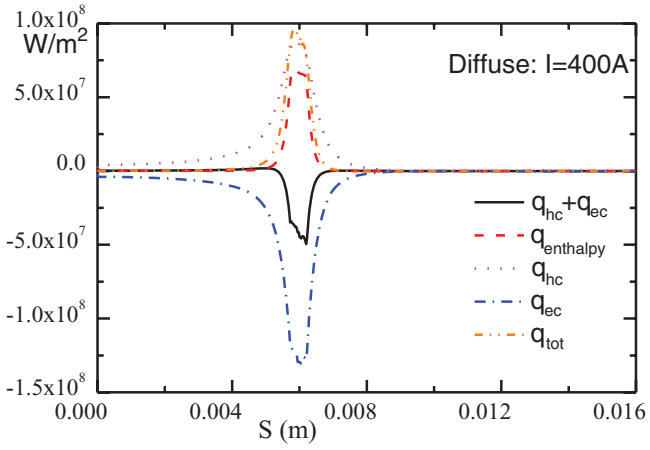

Figure 10. Distributions of the energy flux densities along the cathode surface B–G–F for arc current $I = 400$ A, diffuse mode.

neglect the electrical influence from the bulk plasma for high current arc discharge in the spot mode.

The calculated voltage–current curves are plotted in figure 16 for $I = 50$–600 A, compared with the result from

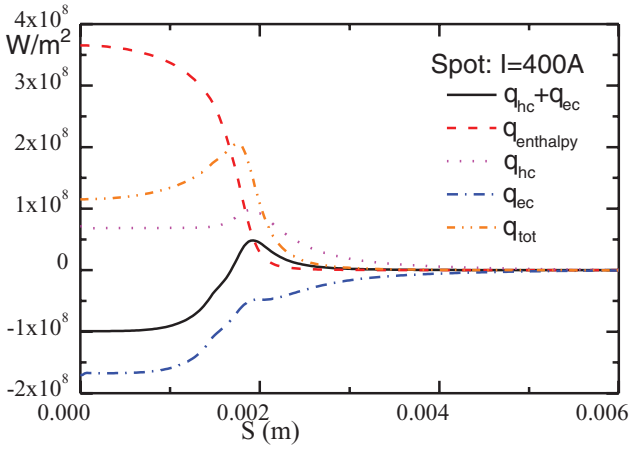

Figure 11. Distributions of the energy flux densities along the cathode surface B–G for arc current $I = 400$ A, spot mode.

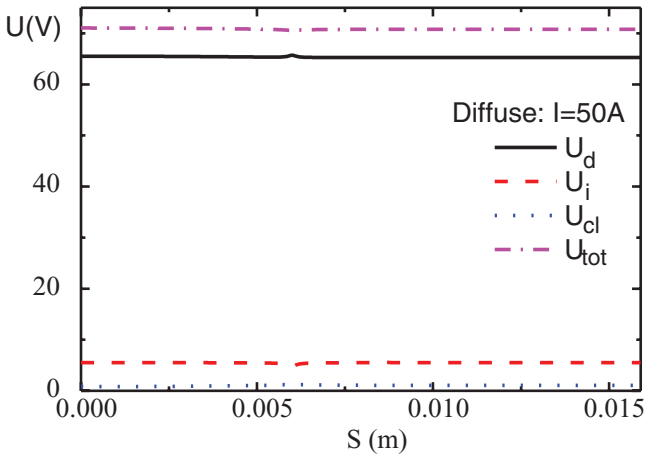

Figure 12. Voltage drops along the cathode surface B–G–F, diffuse mode, $I = 50$ A: $U_d$represents the sheath layer voltage drop; U_i represents the ionization layer voltage drop;U_{cl} represents bulk plasma voltage drop; U_{tot} is the sum of U_i and U_d.

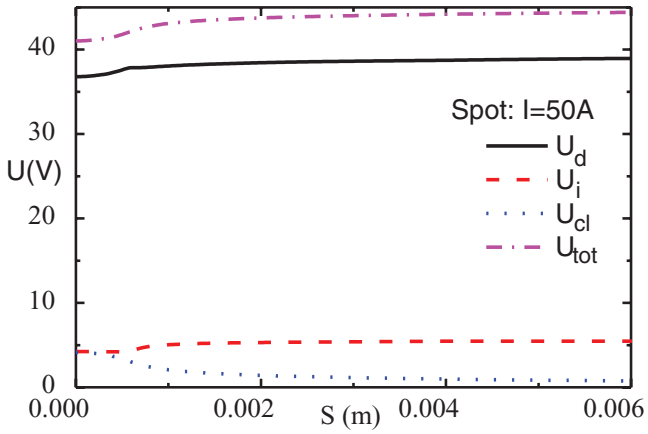

Figure 13. Voltage drop along the cathode surface B–G, spot mode, $I = 50$ A.

the decoupled method [38]. For a certain current, the near-cathode layer voltage drop is not uniform along the cathode surface in the present work. Thus the voltage drops given in figure 16 represent the minimum value of $U_{tot} = U_i + U_d$ (where U_{cl} reaches the maximum) for a certain total current.

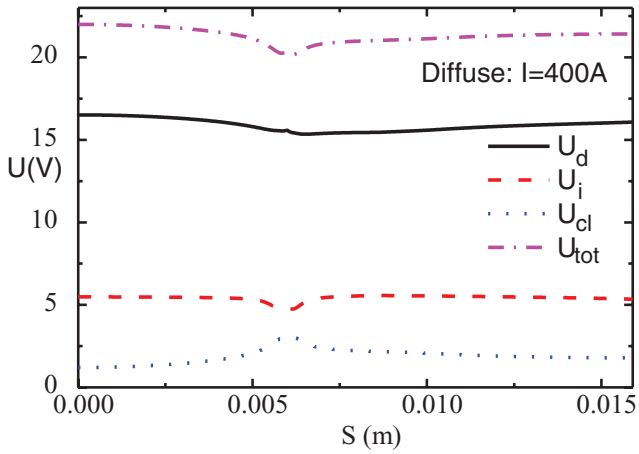

Figure 14. Voltage drop along the cathode surface B–G–F, diffuse mode, $I = 400$ A.

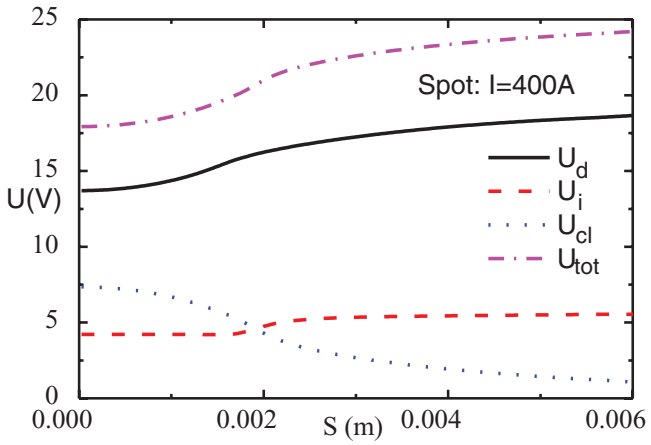

Figure 15. Voltage drop along cathode surface B–G, spot mode, $I = 400$ A.

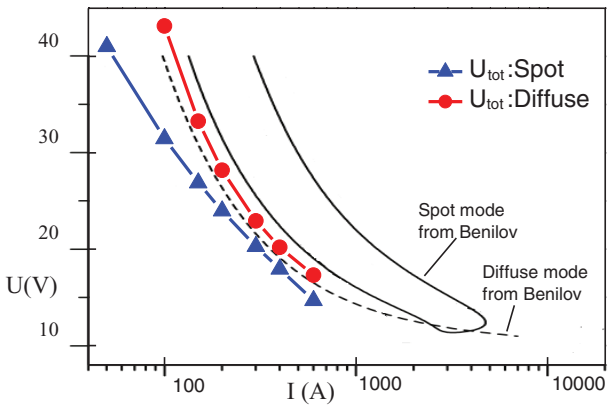

Figure 16. Near-cathode layer voltage drop ($U_i + U_d$) curve as a function of total current for the spot mode and diffuse mode, respectively, compared with results from Benilov [38].

U_{tot} is larger in the diffuse mode than in the spot mode for the same current in this work. However, in Benilov's work, the result is just the opposite, except for a small range of high current. As figure 16 shows, the near-cathode layer voltage drop decreases with the increase of the total current. On the other hand the maximum bulk plasma voltage drop increases with the increase of the total current [25]. Therefore we can speculate that the uniform U_{tot} assumption of the decoupled method should be more physically unrealistic with higher total current in the spot mode.

4. Conclusions

An atmospheric free-burning arc in argon is studied, using the code developed on the basis of a commercial CFD code FLUENT. In this paper the numerical model is based on a previous one [48], which calculates the argon arc simultaneously with the cathode body. The near-cathode layer modeling is coupled with the arc column modeling through setting a transitional layer in the 2D description between them. The arc gap between the cathode and anode is set to 5 mm. The total current is set to 50–600 A. Results are given for a pure tungsten rod cathode of 10 mm length and 6 mm radius.

(a) The thermal emission electrons cools the cathode surface, while the ion flux and back-diffusion plasma electrons heat it.
(b) At the cathode surface, the energy fluxes due to the heat conduction of heavy particles and electrons are comparable to the total heating flux, no matter wether the arc discharge is performed in a high (400 A) or low current (50 A) situation.
(c) Electrical influence from the bulk plasma on the cathode heating modeling becomes essential in the high current situation (>400 A) for the spot mode.
(d) The near-cathode layer voltage drop (U_{tot}) curves are similar to those of the decoupled method. However, U_{tot} is larger in the diffuse mode than in the spot mode for the same current in this work, which is contrary to the results of decoupled modeling.

The results obtained are promising, which indicates that the coupled method of arc modeling differs significantly from the decoupled one. We plan now to work in the following direction: the use of the model in other cathode configurations and in 3D transient state assumption.

Acknowledgments

We thank Dr He-Ping Li (Department of Engineering Physics, Tsinghua University, E-mail: liheping@tsinghua.edu.cn) for careful advice. The discussion with him helped a lot in the writing of this paper.

The work is supported by The National Natural Science Foundation of China: NSFC 11475174, NSFC 11035005, NSFC 50876101.

Appendix A. Sheath and ionization layer

In this section a summary is given of equations describing the near-cathode layer of the plasma. The near-cathode plasma layer comprises two sub-layers: a space-charge sheath, which is adjacent to the cathode surface, and an ionization layer, which is adjacent to the sheath.

The space-charge sheath is considered as collisionless for ions. In the sheath, the ions moving to the cathode and electrons emitted from the cathode are accelerated. The emitted electron flux is found to have an upper limit [61, 62], and the initial energy of the positive ions at their entry plane is found to depend on the emitted electrons.

The ion current flux to the cathode is generated in the ionization layer [63], which is evaluated as:

$$j_{\mathrm{i}} = e n_{\mathrm{i},n} \upsilon_{\mathrm{B}} \tag{A.1}$$

where υ_{B} represents the initial energy of the positive ions at their entry plane of the sheath:

$$\upsilon_{\mathrm{B}}{}^2 = \frac{k_{\mathrm{B}} T_{\mathrm{e}}}{m_{\mathrm{i}}} \left\{ 1 - \mu i_{\mathrm{em}} (\eta_{\mathrm{c}} + \tau)^{-\frac{1}{2}} \left[1 + \frac{1}{2} (\eta_{\mathrm{c}} + \tau)^{-1} \right] \right\}^{-1} \tag{A.2}$$

$n_{\mathrm{i},n}$ represents the ion density at the sheath edge:

$$\frac{n_{\mathrm{i},n}}{n_{\mathrm{i},\infty}} = \frac{\alpha C_2 \sqrt{1+\beta}}{C_2 + 2\alpha C_2 \sqrt{1+\beta} + \alpha^2 \sqrt{1+\beta}} \tag{A.3}$$

$n_{\mathrm{i},\infty}$ is evaluated using the Saha equation for T_{e}, T_{h}, and pressure p (1 atm in this paper) at the interface between ionization layer and thermal perturbation layer. The detailed definitions and calculations of dimensionless coefficients C_2, α and β are given in Benilov's theory of the ionization layer [56, 63]. In addition the detailed definitions and calculations for the dimensionless variables μ, η_{c}, i_{em} and τ are given in the sheath theory for hot cathodes [61, 62].

The current flux of plasma electrons, which come to the cathode surface from the ionization layer after having overcome the retarding electric field in the space-charge sheath, is:

$$j_{\mathrm{bd}} = e n_{\mathrm{p},n} \left(\frac{k_{\mathrm{B}} T_{\mathrm{e}}}{2\pi m_{\mathrm{e}}} \right)^{1/2} \exp\left(-\frac{e U_{\mathrm{d}}}{k_{\mathrm{B}} T_{\mathrm{e}}} \right) \tag{A.4}$$

where $n_{\mathrm{p},n} = n_{\mathrm{i},n} - \frac{j_{\mathrm{em}}}{e} (m_{\mathrm{e}})^{\frac{1}{2}} (2eU_{\mathrm{d}} + 2k_{\mathrm{B}} T_{\mathrm{ca}})^{-\frac{1}{2}}$, represents the density of plasma electrons at the sheath edge. U_{d} represents the sheath voltage drop.

The electron emission current flux from the cathode surface by means of the Richardson–Schottky formula reads:

$$j_{\mathrm{em}} = e A_j T_{\mathrm{ca}}^2 \exp\left(-\frac{A - \Delta A}{k_{\mathrm{B}} T_{\mathrm{ca}}} \right) \tag{A.5}$$

where $\Delta A = \sqrt{\frac{e^3 E_{\mathrm{c}}}{4\pi\varepsilon_0}}$ is the Schottky correction to A, the work function for the thermionic emission of the electrode surface. E_{c}, i.e. the electric field at the cathode surface, is obtained by solving Poisson's equation in the sheath zone [61]:

$$\begin{aligned} \frac{1}{2} \frac{\varepsilon_0}{n_{\mathrm{i},n} k_{\mathrm{B}} T_{\mathrm{e}}} (E_{\mathrm{c}})^2 = {} & 2\eta_0 \left[\left(1 + \frac{\eta_{\mathrm{c}}}{\eta_0} \right)^{\frac{1}{2}} - 1 \right] \\ & - \left[1 - \mu i_{\mathrm{em}} (\eta_{\mathrm{c}} + \tau)^{-\frac{1}{2}} \right] (1 - \mathrm{e}^{-\eta_{\mathrm{c}}}) \\ & - 2\mu i_{\mathrm{em}} \left[(\eta_{\mathrm{c}} + \tau)^{\frac{1}{2}} - \tau^{\frac{1}{2}} \right] \end{aligned} \tag{A.6}$$

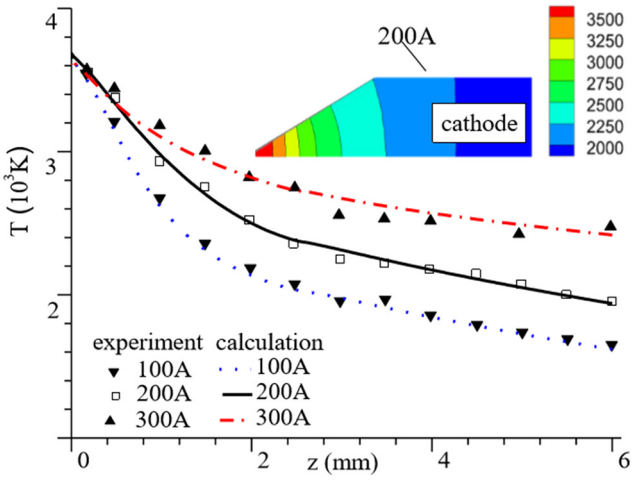

Figure B1. A comparison of the predicted temperatures of the cathode surface with the experimental measurement of Haidar and Farmer [1]: thoriated tungsten cathode with a 60° conical tip, arc current $I = 100$ A, 200 A, 300 A. z represents the axial distance from the cathode tip.

ε_0 is the dielectric constant, and η_0 is a dimensionless variable [61].

In the solution process, if the right-hand side of equation (6) is smaller than zero, j_{em} is evaluated as:

$$j_{\mathrm{em}} = e n_{\mathrm{i},n} \sqrt{\frac{2k_{\mathrm{B}} T_{\mathrm{e}}}{m_{\mathrm{i}}}} \frac{2\eta_0 \left[\left(1 + \frac{\eta_{\mathrm{c}}}{\eta_0} \right)^{\frac{1}{2}} - 1 \right] - (1 - \mathrm{e}^{-\eta_{\mathrm{c}}})}{2\mu \left[(\eta_{\mathrm{c}} + \tau)^{\frac{1}{2}} - \tau^{\frac{1}{2}} \right] - \mu (\eta_{\mathrm{c}} + \tau)^{-\frac{1}{2}} (1 - \mathrm{e}^{-\eta_{\mathrm{c}}})}. \tag{A.7}$$

The voltage drop in the ionization layer U_{i} and the sheath voltage drop U_{d} are evaluated as:

$$U_{\mathrm{i}} = \frac{k_{\mathrm{B}} T_{\mathrm{e}}}{e} \ln \frac{n_{\mathrm{i},\infty}}{n_{\mathrm{i},n}}, \quad U_{\mathrm{d}} = U_{\mathrm{tot}} - U_{\mathrm{i}}. \tag{A.8}$$

Here U_{tot} is the given total voltage drop.

One can see that the near-cathode layer description in this paper mainly combines the ionization layer theory of Benilov [56, 63] and the hot cathode theory of Askari *et al* [61, 62]. Benilov also developed a double sheath theory [34, 64] in which the electron emission does not influence the sheath electric field. In Benilov's theory, the Bohm velocity is evaluated as $\upsilon_{\mathrm{B}} = \sqrt{\frac{k_{\mathrm{B}}(T_{\mathrm{e}} + T_{\mathrm{h}})}{m_{\mathrm{i}}}}$, different from equation (2). This evaluation equals equation (2), when $T_{\mathrm{e}}/T_{\mathrm{h}}$ is taken as $+\infty$ and j_{em} is taken as zero.

Appendix B. Comparison with experimental results

B.1. Case 1

To apply and examine our coupling model (thermal perturbation (TP)-sheath model), a typical free burning arc configuration (thoriated tungsten cathode with a 60 ° conical tip, arc gap 5 mm) was chosen, which corresponds to the conditions of experiment [1] and is in agreement with previous studies

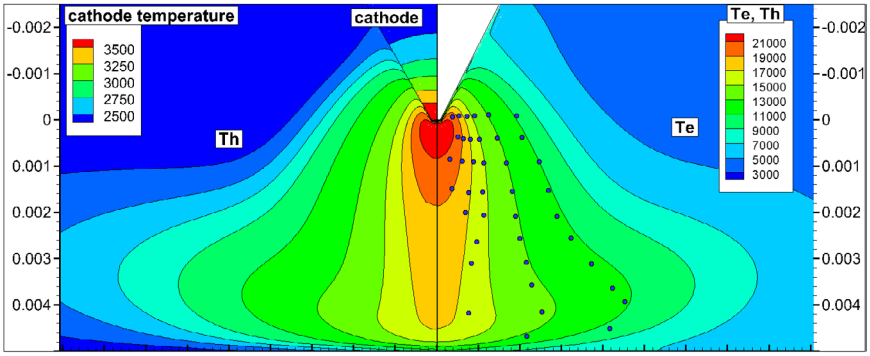

Figure B2. The predicted temperature contours for a 200 A arc compared with the experimental points of Haddad and Farmer [22].

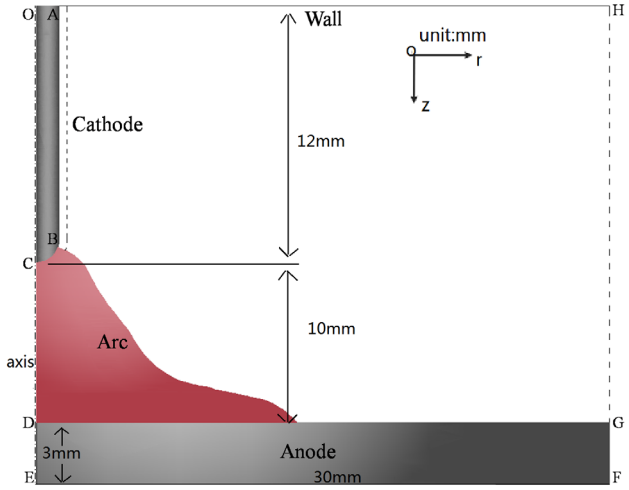

Figure B3. The sketch of the geometry.

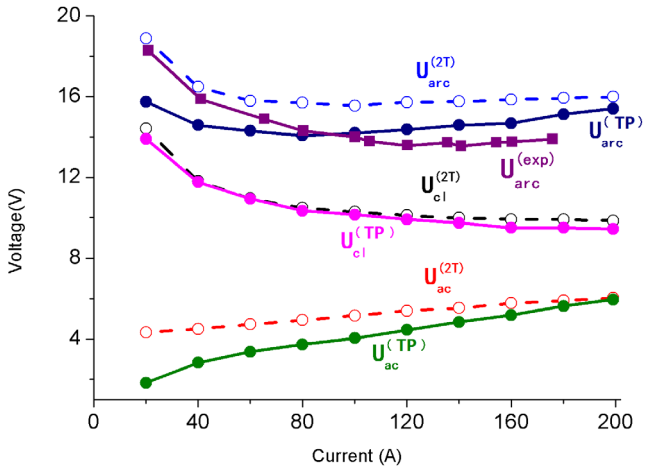

Figure B4. $U_{ac}^{(TP)}$, $U_{ac}^{(2T)}$: the arc column voltage predicted by, respectively, the TP-sheath model and the 2T-sheath model. $U_{cl}^{(TP)}$, $U_{cl}^{(2T)}$: the near cathode layer voltage drop predicted by the TP-sheath model and the 2T-sheath model. $U_{arc}^{(TP)}$, $U_{arc}^{(2T)}$: the total arc voltage predicted by the TP-sheath model and the 2T-sheath model. $U_{arc}^{(exp)}$: arc voltage measured by the experiment.

[21, 22]. In the present model, the arc plasmas are divided into five regions: the solid cathode body, sheath, pre-sheath, arc column and the solid anode body. The anode sheath is neglected and the anode body is coupled with the arc column by setting a heat flux to the anode surface [21].

Figure B1 shows the comparison of calculated temperatures at the cathode surface and the experimental measurements from the literature [1]. The electron temperature and heavy particle temperature of the arc column are plotted in figure B2, compared with experimental points of Haddad and Farmer [22]. It can be seen that the calculated temperatures for different arc currents (100 A, 200 A and 300 A) are all in good agreement with the experimental data. The comparison of calculated values and experimental data proved that our coupling model is practical.

B.2. Case 2

The numerical simulations performed using the 2T-sheath model (a 2T bulk plasma in ionization equilibrium, with near-cathode layer modeling including a space charge layer) under the conditions of the experiment in [5] were reported in [25]. In this work, the numerical simulations under the same conditions are carried out by means of the TP-sheath mode. In addition, a comparison between the results of the two models is given in this section.

A sketch of the geometry is shown in figure B3. The cathode in the calculation domain is a cylinder made of tungsten with a hemispherical tip. The water-cooled anode is flat and made of copper. The bottom of the cathode and the outer part of the anode are considered to have an ambient temperature of 300 K. The arc chamber is closed. The current performed in this work is in the range 20–200 A.

The predicted arc column voltage U_{ac}, the near cathode layer voltage drop U_{cl} and the total arc voltage U_{arc} ($U_{arc} = U_{ac} + U_{cl}$) calculated by means of the TP-sheath model and the 2T-sheath model are shown in figure B4. Experimental data of the arc voltage taken from [5] are also shown in figure B4. There are two forms of arc attachment in the experiment [5]: diffuse and contracted. However, the values of the arc voltage in the two forms do not differ significantly. Note that the values shown in figure 6 belong to the diffuse form. We can see that the values of the arc voltage first decrease with increasing current and then increase slightly in both the TP-sheath and 2T-sheath models, which is due to the decrease in the near cathode layer voltage drop and the increase in the voltage of the arc column with increasing current. These numerical results of the two models are not very different from each other and from the

experiment: the difference is below 2V at both low current and high current. The near cathode layer voltage drop calculated by the TP-sheath model is very similar to the one calculated by the 2T-sheath model. The values of the arc column voltage predicted by the two models are more different, especially in the case of lower currents. However, the difference does not exceed 2 V, even at low current.

References

[1] Haidar J and Farmer A J D 1995 Surface-temperature measurements for tungsten-based cathodes of high-current free-burning arcs *J. Phys. D: Appl. Phys.* **28** 2089–94

[2] Redwitz M, Langenscheidt O and Mentel J 2005 Spectroscopic investigation of the plasma boundary layer in front of HID-electrodes *J. Phys. D: Appl. Phys.* **38** 3143–54

[3] Nemchinsky V 2003 Current density at the refractory cathode of a high-current high-pressure arc (two modes of cathode spot attachment) *J. Phys. D: Appl. Phys.* **36** 3007–13

[4] Dabringhausen L, Langenscheidt O, Lichtenberg S, Redwitz M and Mentel J 2005 Different modes of arc attachment at HID cathodes: simulation and comparison with measurements *J. Phys. D: Appl. Phys.* **38** 3128–42

[5] Mitrofanov N K and Shkol'nik S M 2007 Two forms of attachment of an atmospheric-pressure direct-current arc in argon to a thermionic cathode *Tech. Phys.* **52** 711–20

[6] Nandelstadt D, Luhmann J and Mentel J 1999 Measuring the power losses of thermionic arc cathodes *Int. Conf. on Phenomena in Ionized Gas Proc.* vol 1 pp 15–6

[7] Tashiro S, Tanaka M and Murphy A B 2010 Numerical analysis of non-equilibrium plasma property in anode boundary layer of argon gas tungsten arc *Surf. Coat. Technol.* **205** S115–9

[8] Tanaka M, Terasaki H and Ushio M 2002 Effect of anode heat transfer on melted penetration in welding process by free-burning argon arc *Isij. Int.* **42** 1005–9

[9] Tanaka M, Ushio M and Wu C S 1999 One-dimensional analysis of the anode boundary layer in free-burning argon arcs *J. Phys. D: Appl. Phys.* **32** 605–11

[10] Tanaka M and Ushio M 1999 Observations of the anode boundary layer free-burning argon arcs *J. Phys. D: Appl. Phys.* **32** 906–12

[11] Tanaka M and Ushio M 1999 Plasma state in free-burning argon arc and its effect on anode heat transfer *J. Phys. D: Appl. Phys.* **32** 1153–62

[12] Dinulescu H A and Pfender E 1980 Analysis of the anode boundary-layer of high-intensity arcs *J. Appl. Phys.* **51** 3149–57

[13] Almeida N A, Benilov M S and Naidis G V 2008 Unified modelling of near-cathode plasma layers in high-pressure arc discharges *J. Phys. D: Appl. Phys.* **41** 4036–2

[14] Hsu K C and Pfender E 1983 2-temperature modeling of the free-burning, high-intensity arc *J. Appl. Phys.* **54** 4359–66

[15] Bai B 2012 The simulation of magnetically dispersed arc plasma coupled with electrode *Thermal Science and Engneering* (Hefei: University of Science and Technology of China)

[16] Chen T, Zhang X N, Bai B, Xu Z M, Wang C and Xia W D 2015 Numerical Study of DC argon arc with axial magnetic fields *Plasma Chem. Plasma Process.* **35** 61–74

[17] Wang C, Chen T, Li W W, Zha J and Xia W D 2014 Axial magnetic field effects on xenon short-arc lamps *Plasma Sci. Technol.* **16** 1096–9

[18] Xia W D, Li L C, Zhao Y H, Ma Q, Du B H, Chen Q and Cheng L 2006 Dynamics of large-scale magnetically rotating arc plasmas *Appl. Phys. Lett.* **88** 211501–3

[19] Bai B, Zha J, Zhang X M, Wang C and Xia W D 2012 Simulation of magnetically dispersed arc plasma *Plasma Sci. Technol.* **14** 118–21

[20] Zhou H L, Zhou Z P, Li L C, Cheng L, Bai B and Xia W D 2008 Investigation of a novel large area dispersed arc plasma source with time-resolved ICCD Imaging *IEEE Trans. Plasma Sci.* **36** 1082–3

[21] Sansonnens L, Haidar J and Lowke J J 2000 Prediction of properties of free burning arcs including effects of ambipolar diffusion *J. Phys. D: Appl. Phys.* **33** 148–57

[22] Lowke J J, Morrow R and Haidar J 1997 A simplified unified theory of arcs and their electrodes *J. Phys. D: Appl. Phys.* **30** 2033–42

[23] Zhu P Y, Lowke J J and Morrow R 1992 A unified theory of free burning arcs, cathode sheaths and cathodes *J. Phys. D: Appl. Phys.* **25** 1221–30

[24] Lowke J J, Kovitya P and Schmidt H P 1992 Theory of free-burning arc columns including the influence of the cathode *J. Phys. D: Appl. Phys.* **25** 1600–6

[25] Benilov M S, Benilova L G, Li H P and Wu G Q 2012 Sheath and arc-column voltages in high-pressure arc discharges *J. Phys. D: Appl. Phys.* **45** 629–36

[26] Li H P and Benilov M S 2007 Effect of a near-cathode sheath on heat transfer in high-pressure arc plasmas *J. Phys. D: Appl. Phys.* **40** 2010–7

[27] Murphy A B 2011 A self-consistent three-dimensional model of the arc, electrode and weld pool in gas-metal arc welding *J. Phys. D: Appl. Phys.* **44** 252–60

[28] Murphy A B, Tanaka M, Tashiro S, Sato T and Lowke J J 2009 A computational investigation of the effectiveness of different shielding gas mixtures for arc welding *J. Phys. D: Appl. Phys.* **42** 115205

[29] Schnick M, Fuessel U, Hertel M, Spille-Kohoff A and Murphy A B 2011 Numerical investigations of arc behaviour in gas metal arc welding using ANSYS CFX *Front. Mater. Sci.* **5** 98–108

[30] Schnick M, Fussel U, Hertel M, Spille-Kohoff A and Murphy A B 2010 Metal vapour causes a central minimum in arc temperature in gas-metal arc welding through increased radiative emission *J. Phys. D: Appl. Phys.* **43** 22001–5

[31] Schnick M, Fuessel U, Hertel M, Haessler M, Spille-Kohoff A and Murphy A B 2010 Modelling of gas-metal arc welding taking into account metal vapour *J. Phys. D: Appl. Phys.* **43** 2460–8

[32] Benilov M S, Almeida N A, Baveva M, Cunha M D and Benilova L G 2016 Account of near-cathode sheath in numerical models of high-pressure arc discharges *J. Phys. D: Appl. Phys.* **49** 215201

[33] Baeva M, Benilov M S, Almeida N A and Uhrlandt D 2016 Novel non-equilibrium modelling of a DC electric arc in argon *J. Phys. D: Appl. Phys.* **49** 245205

[34] Benilov M S and Marotta A 1995 A model of the cathode region of atmospheric-pressure arcs *J. Phys. D: Appl. Phys.* **28** 1869–82

[35] Paul K C, Takemura T, Hiramoto T, Erraki A, Dawson F, Zissis G, Gonzalez J J, Gleizes A, Benilov M S and Lavers J D 2006 Self-consistent model of HID lamp for design applications *IEEE Trans. Plasma Sci.* **34** 1536–47

[36] Botticher R and Botticher W 2001 Numerical modelling of a dynamic mode change of arc attachment to cathodes of high-intensity discharge lamps *J. Phys. D: Appl. Phys.* **34** 1110–5

[37] Botticher R and Botticher W 2000 Numerical modelling of arc attachment to cathodes of high-intensity discharge lamps *J. Phys. D: Appl. Phys.* **33** 367–74

[38] Benilov M S and Cunha M D 2003 Heating of refractory cathodes by high-pressure arc plasmas: II *J. Phys. D: Appl. Phys.* **36** 603–14

[39] Benilov M S and Cunha M D 2002 Heating of refractory cathodes by high-pressure arc plasmas: I *J. Phys. D: Appl. Phys.* **35** 1736–50
[40] Benilov M S 1998 Nonlinear surface heating of a plane sample and modes of current transfer to hot arc cathodes *Phys. Rev.* E **58** 6480–94
[41] Baeva M, Kozakov R, Gorchakov S and Uhrlandt D 2012 Two-temperature chemically non-equilibrium modelling of transferred arcs *Plasma Sources Sci. Technol.* **21** 1020–7
[42] Coulombe S and Meunier J L 1997 Arc-cold cathode interactions: parametric dependence on local pressure *Plasma Sources Sci. Technol.* **6** 508–17
[43] Coulombe S and Meunier J L 2000 Theoretical prediction of non-thermionic arc cathode erosion rate including both vaporization and melting of the surface *Plasma Sources Sci. Technol.* **9** 239–47
[44] Bade W L and Yos Y M 1963 Theoretical and experimental study of thermionic arc cathodes *Technical Documentary Report* (Wilmington, MA: Research and Development Division, Avco Corporation)
[45] Neumann W 1969 Der katodenmechanismus von Hochbruckbogen Beitr Plasmaphysik *Beitr. Plasmaphysik* **9** 499–526
[46] Nemchinsky V 2004 Heat flux at the refractory cathode of a high-current, high-pressure arc (two modes of cathode spot attachment) *J. Phys. D: Appl. Phys.* **37** 1048–51
[47] Lichtenberg S, Dabringhausen L, Langenscheidt O and Mentel J 2005 The plasma boundary layer of HID-cathodes: modelling and numerical results *J. Phys. D: Appl. Phys.* **38** 3112–27
[48] Chen T, Wang C, Liao M R and Xia W D 2016 Diffuse and spot mode of cathode arc attachments in an atmospheric magnetically rotating argon arc *J. Phys. D: Appl. Phys.* **49** 085202
[49] Benilov M S 2001 Near-cathode phenomena in HID lamps *IEEE Trans. Ind. Appl.* **37** 986–3
[50] Nemchinsky V 2013 What determines current density at the cathode of a thermionic arc? *J. Phys. D: Appl. Phys.* **46** 255202–9
[51] Nemchinsky V A and Raitses Y 2015 Atmospheric pressure arc discharge with ablating graphite anode *J. Phys. D: Appl. Phys.* **48** 1–18
[52] Nemchinsky V 2015 Heat transfer to a cathode of a rotating arc *Plasma Sources Sci. Technol.* **24** 035013
[53] Nemchinsky V 2014 Arc discharge anode reattachment: simple model *IEEE Trans. Plasma Sci.* **42** 4026–30
[54] Benilov M S 2008 Understanding and modelling plasma-electrode interaction in high-pressure arc discharges: a review *J. Phys. D: Appl. Phys.* **41**
[55] Baeva M, Bosel A, Ehlbeck J and Loffhagen D 2012 Modeling of microwave-induced plasma in argon at atmospheric pressure *Phys. Rev.* E **85** 4001–14
[56] Benilov M S 1995 The ion flux from a thermal plasma to a surface *J. Phys. D: Appl. Phys.* **28** 286–94
[57] Gonzalez J J, Lago F, Freton P, Masquere M and Franceries X 2005 Numerical modelling of an electric arc and its interaction with the anode: part II. The three-dimensional model—influence of external forces on the arc column *J. Phys. D: Appl. Phys.* **38** 306–18
[58] Zhang X N, Li H P, Murphy A B and Xia W D 2013 A numerical model of non-equilibrium thermal plasmas. I. Transport properties *Phys. Plasmas* **20** 033508
[59] Moizhes B Y and Nemchinsky V A 1976 Theory of the cylindrical cathode in a high pressure arc *Sov. Phys. Techn. Phys.* **20** 757–62
[60] Benilov M S 2014 Multiple solutions in the theory of dc glow discharges and cathodic part of arc discharges. Application of these solutions to the modeling of cathode spots and patterns: a review *Plasma Sources Sci. Technol.* **23** 054019
[61] Askari S and Minoo H 2008 Analytical expression for the electric potential in the plasma sheath near an arc-cathode *Phys. Plasmas* **15** 043503
[62] Prewett P D and Allen J E 1976 The double sheath associated with a hot cathode *Proc. R. Soc.* A **348** 435–66
[63] Benilov M S and Naidis G V 1998 Ionization layer at the edge of a fully ionized plasma *Phys. Rev.* E **57** 2230–41
[64] Benilov M S and Benilova L G 2010 The double sheath on cathodes of discharges burning in cathode vapour *J. Phys. D: Appl. Phys.* **43** 227–38